# Metal dicarboxylates as anode materials for Li-ion batteries – Supporting information

Authors: Matthew Teusner[a*], Jitendra Mata[b], Bernt Johannessen[c], Glen Stewart[d], Seán Cadogan[d], Neeraj Sharma[a].

[a] School of Chemistry, The University of New South Wales, Kensington, NSW 2052, Australia.

[b]Australian Centre for Neutron Scattering (ACNS), Australia's Nuclear Science and Technology Organisation (ANSTO), Lucas Heights, NSW 2234, Australia.

[c]Australian Synchrotron, ANSTO, 800 Blackburn Rd, Clayton VIC 3168.

[d] School of Science, The University of New South Wales, Australian Defence Force Academy, Canberra, ACT 2600, Australia.

[*] Corresponding author

# Experimental

## Metal-acid synthesis

The general method for the synthesis of the metal-acid species is detailed below. Some of the syntheses required modification to the general synthesis parameters to achieve practical yields or increase ease of product recovery i.e. decrease product solubility in the reaction mixture. In the case of the iron-tartaric acid reaction, the synthesis conditions listed below produced a crystalline product which increased ease of characterisation. The specific reaction conditions for each species are summarised in Table 1. The additional reaction condition variations for the copper tartrate syntheses are detailed in the Table 2.

Powders of the chosen metal (10 mmol) and acid (10 mmol) were stirred overnight in an NMP/water solution (50 mL) at 66 - 80 $^{o}$C. The following day, the reaction mixture was filtered and the collected solid was washed with NMP and acetone, followed by drying under vacuum at 100 $^{o}$C. For the copper- tartaric acid reaction, both the hydrous (green) and anhydrous (blue) analogues were isolated as an insoluble solid from the reaction mixture. After collection by filtration, the solid was dispersed in water which dissolved the hydrous analogue. The insoluble copper tartrate was collected by filtration and the hydrous analogue was recovered by evaporation of the water under reduced pressure. L-tartaric and D,L-malic acid were used for the relevant syntheses.

*Table 1: Summary of the synthesis parameters for each metal-acid reaction undertaken in this study. Yield calculations are approximate due to plausible impurities and, where the exact chemical formula is unknown, based on the assumed chemical formula (as discussed in the main text).*

| | NMP/water ratio | Temperature / °C | Approximate yield / % |
|---|---|---|---|
| **Copper-tartaric acid** | 1:0 | 70 | 22 (Cu TAR hydrous)<br>61 (Cu TAR) |
| **Copper- malic acid** | 1:1 | 80 | 44 |
| **Copper-maleic acid** | 1:1 | 79 | 63 |
| **Iron-tartaric acid** | 1:9 | 77 | 81 |
| **Iron-malic acid** | 1:1 | 70 | 74 |
| **Iron-maleic acid** | 1:1 | 66 | 56 |
| **Zinc-tartaric acid** | 1:1 | 68 | 79 |
| **Zinc-malic acid** | 1:1 | 68 | 59 |
| **Zinc-maleic acid** | 1:1 | 70 | 84 |

*Table 2: Summary of the synthesis parameter variations for the copper tartrate syntheses*

| | Temperature / °C | Reaction time | Solvent |
|---|---|---|---|
| 1 | RT | 3 days | NMP |
| 2 | 90 | Overnight | NMP |
| 3 | 70 | 3 days | Water |
| 4 | 70 | Overnight | 9:1 NMP/water |
| 5 | 70 | Overnight | 1:1 NMP/water |

## Electrode formulation and electrochemical tests

To make the NMP-based electrodes, a slurry was prepared using a 5:4:1 ratio of the metal-acids, conductive carbon black and polyvinylidene difluoride (PVDF) binder in N-methyl pyrrolidone (NMP), which was magnetically stirred overnight. To make the water-based electrodes, a slurry was prepared using a 5:4:1 ratio of the metal-acids, conductive carbon and 2:3 carboxymethyl cellulose (CMC)/ styrene butadiene rubber (SBR) in water, which was magnetically stirred overnight. For the water-based carbon black electrode, a 9:1 conductive carbon to CMC/SBR slurry was made.

The slurry was spread onto a copper foil current collector at 100 µm thickness using a notch bar, resulting in an active material loading of approximately 0.8 – 1.4 $mgcm^{-2}$. The electrode sheets were dried overnight in a vacuum oven at 100 $^{o}C$ under dynamic vacuum. After drying, the electrodes were pressed for an hour at 100 $kNm^{-2}$ using a flat plate press (MTI corporation) to ensure good contact between the anode mixture and the substrate. For the creation of coin cells, 12 mm anode discs were punched from the electrode sheet and dried for an hour at 100 $^{O}C$ under dynamic vacuum to remove any residual moisture before transferring into an Ar-filled glovebox for cell assembly. CR2032 coin cells were assembled, with a glass-fibre separator soaked in electrolyte, and Li was used as the counter electrode. The electrolyte used was 1 M $LiPF_6$ in 1:1 ethylene carbonate (EC)/dimethyl carbonate (DMC).

For the galvanostatic cycling tests, the coin cells were discharged and charged at 50 $mAg^{-1}$ between 0.01-3 V using a cell cycler system (Neware BTS3000 or LANDT BTS CT3002A). Rate capability tests were conducted starting at 50 $mAg^{-1}$, with doubling current density, up to 6400 $mAg^{-1}$, before returning to 50 $mAg^{-1}$. 5 cycles were conducted at each current density, with cycling between 0.01 and 3 V.

## Metal-acid and electrode characterisation

X-ray diffraction (XRD) data were collected using a PANalytical Xpert Multipurpose X-ray Diffraction System at the Mark Wainwright Analytical Centre, UNSW. The instrument was operated at a voltage

of 45 kV and current of 40 mA, employing Cu $K_\alpha$ (λ = 1.54 Å) radiation with step size of 0.013 ° in the range 10 < 2θ° < 40.

Single crystals were formed by dissolving the metal-acid (~ 10 mg) in water (~ 2 mL). The resulting solutions were left to evaporate at room temperature until no visible water remained.

A plate-like single crystal with dimensions of 50 - 150 μm was selected under the polarizing microscope (Leica M165Z), and it was then mounted on a MicroMount (MiTeGen, USA), consisting of a thin polymer tip with a wicking aperture. The X-ray diffraction measurements were carried out on a Bruker D8 Quest Single Crystal diffractometer with a Photon II detector at 120 K by using IμS 3.0 Microfocus Source with Mo-$K_\alpha$ radiation (λ = 0.710723 Å). The single crystal was coated with NVH immersion oil and then quickly transferred to the cold nitrogen stream using the Oxford Cryostream 800 series attachment, and it was mounted on the goniometer using a cryo loop for intensity measurement. Symmetry related absorption corrections using the program SADABS[1] were applied and the data were corrected for Lorentz and polarisation effect using Bruker APEX4 software. The structure was solved by ShelxT (intrinsic phasing)[2] and the full-matrix least-squares refinement was carried out using Shelxl[3] in Olex2[4]. The non-hydrogen atoms were refined anisotropically. The molecular image was generated using Olex2 program[4].

X-ray photoelectron spectroscopy (XPS) was performed on a Thermo Scientific ESCALAB250Xi, using mono-chromated Al-$K_\alpha$ (energy 1486.68 eV). Scanning electron microscopy (SEM) was performed using a Hitachi TM4000 at 15 kV in back scattered electron (BSE) mode. Fourier transform infrared (FTIR) spectroscopy was conducted using a Nicolet iS5. Thermogravimetric analysis (TGA) was conducted using a Netzsch STA 449 F1 Jupiter, under 200 mL/min synthetic air (80:20 nitrogen/oxygen) using an alumina crucible and a heating rate of 10 $^oC$/min.

Room temperature $^{57}$Fe-Mössbauer spectra were recorded in transmission geometry using a commercial Rh matrix $^{57}$Co source (≈25 mCi) mounted on a sinusoidal motion transducer. The powdered specimen material (typically about 190 mg) was mounted between thin, 2.5 cm diameter, beryllium disks. No additional filler material was required. Data were collected over 1024 channels (which on folding resulted in 512 channels) and the velocity was calibrated against the room temperature magnetic spectrum recorded for α-Fe under the same conditions. All spectra were least-squares fitted to Lorentzian components.

Small angle neutron scattering (SANS) measurements were carried out on QUOKKA, [5] and ultra-small-angle neutron scattering (USANS) measurements were carried out on KOOKABURRA[6] both at the Australian Nuclear Science and Technology Organisation (ANSTO), Lucas Heights, Australia. 100 µm electrodes were prepared on copper and aluminium foil (using the previously mentioned method) and the samples were mounted on the front face of sample holder. Sample thickness (copper + electrode) was taken as 100 µm for the purposes of intensity scaling. SANS scattering data were radially averaged (under the assumption of isotropic scattering) and placed on an absolute scale using the direct beam intensity. These absolute intensities were plotted against the scattering vector q. The value of q was defined as:

$$q = \frac{4\pi sin\theta}{\lambda}$$

where λ is the wavelength of the incident neutron beam and 2θ is the scattering angle. For SANS, neutrons with wavelengths of 5 and 8.1 Å were used and data were collected on two-dimensional detectors positioned at 1.3 (with 300 mm offset with 12 m of neutron collimation), 12 (with 12 m of neutron collimation) and 20 (lens optic with 8.1 Å with 20 m of neutron collimation) m from the sample. For USANS, neutrons with a wavelength of 4.74 Å were used. USANS data were converted to absolute scale and then de-smeared using the Lake algorithm incorporated in NIST USANS macros to combine with SANS data[7]. The SANS and USANS data were combined using Igor Pro. To help

highlight the difference between the NMP and water based electrode data, the water based electrode data was divided by the NMP based electrode data.

Fe K-edge X-ray absorption spectroscopy (XAS) measurements were conducted on the MEX bending magnetic beamline at the Australian Synchrotron equipped with a double-crystal Si(111) monochromator and collimating and focusing mirrors. Samples were prepared as extracted electrodes mounted and sealed onto sample holders with Kapton tape in an Ar-filled glove box prior to measurements. XAS data were collected in transmission mode using a set of Iontech gridded and sealed (He) ion chambers and with samples housed in a Helium filled sample stage at room temperature. A bulk metallic Fe foil was used for concurrent energy calibration and monitoring. Data normalisation and analysis was performed using the Demeter software package [Ravel, B.; Newville, M., ATHENA, ARTEMIS, HEPHAESTUS: data analysis for X-ray absorption spectroscopy using IFEFFIT[8].

# Supplementary information

## Synthesis conditions (NMP/$H_2O$)

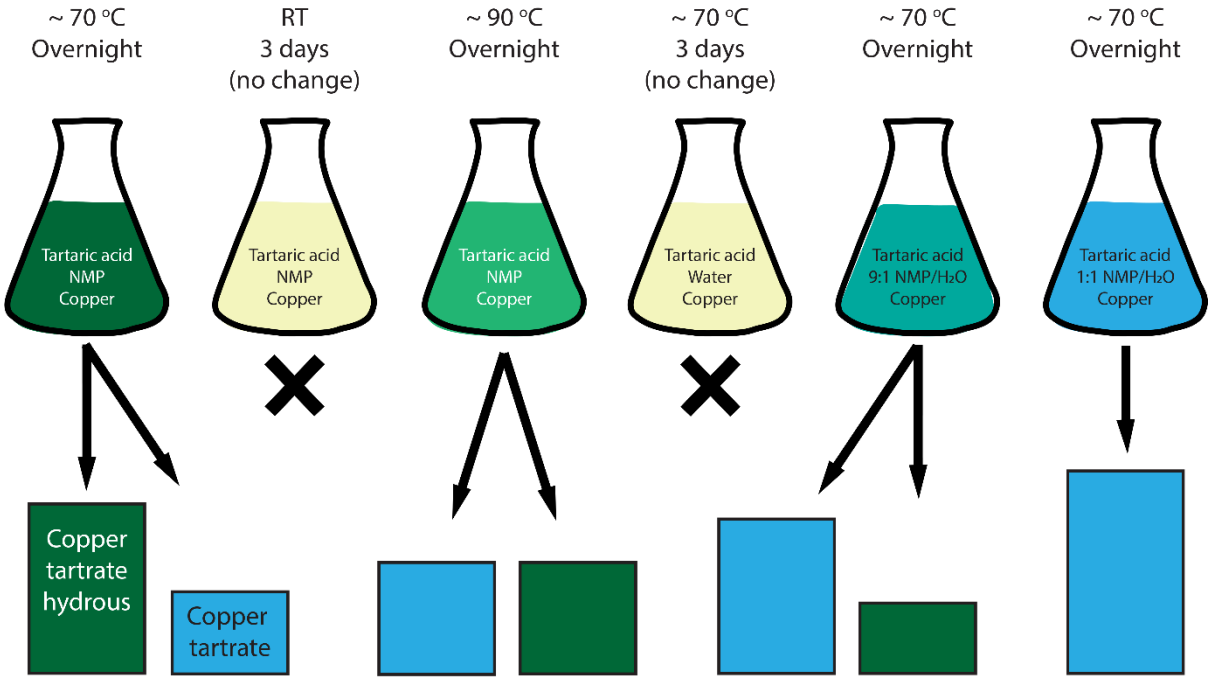


*Figure S1: Representation of the products produced when varying the synthesis parameters of the copper-tartaric acid reaction. Green boxes represent copper tartrate hydrous, and blue boxes represent copper tartrate and the relative sizes are an approximation of the relative quantites produced by the different reactions.*

The synthesis conditions were varied to model how the electrode formulation might affect the product formation, i.e. the ratio of copper tartrate and copper tartrate hydrous, or even the nature of the species formed (Figure S1, Table S1). Previously, both the electrode drying temperature/time and the slurry solvent were shown to play a role in the copper-acid reaction outcome and subsequently the electrode nano and microstructure[9-10]. As expected, no reaction was observed both when the reaction was not heated (reaction 2), and when the solvent used was water (reaction 4). Increasing the reaction temperature from 70 to 90 °C (reaction 1 and 3 respectively) resulted in a more equal ratio of the two products, i.e. increase/decrease in generation of copper tartrate and copper tartrate hydrous respectively. Inclusion of water in the reaction solvent resulted in an increase in the production of copper tartrate; 10% $H_2O$ (reaction 5) resulted in copper tartrate becoming the major product, and 50% $H_2O$ resulted in only copper tartrate being produced. Ultimately, this further demonstrates that the electrode formulation conditions affect the outcome

of the *in-situ* copper-acid reaction, likely allowing rational tailoring of the electrode microstructure through control of the reaction.

*Table S1: Summary of the synthesis parameters for the copper-acid reactions*

| **Reaction number** | **1** | **2** | **3** | **4** | **5** | **6** |
|---|---|---|---|---|---|---|
| **Solvent** | NMP | NMP | NMP | Water | 9:1 NMP/$H_2O$ | 1:1 NMP/$H_2O$ |
| **Temperature / ºC** | 70 | Ambient | 90 | 70 | 70 | 70 |
| **Time** | Overnight | 3 days | Overnight | 3 days | Overnight | Overnight |
| **Major product** | Cu TAR hydrous | No product | Equal | No product | Cu TAR | Only Cu TAR |

## Supplementary data

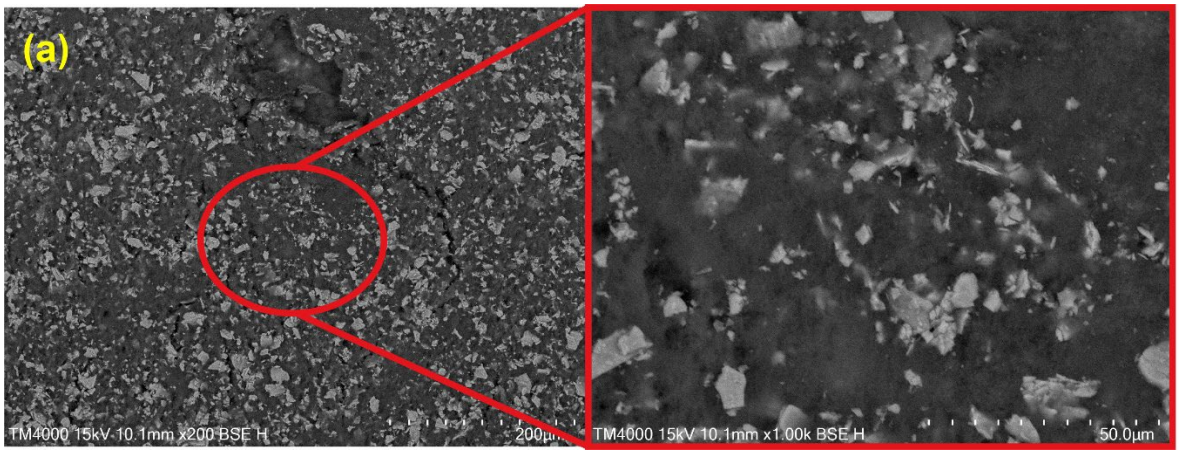


*Figure S2: (a) SEM (200/1000x, 15 kV) of pristine $H_2O$ based copper tartrate electrode.*

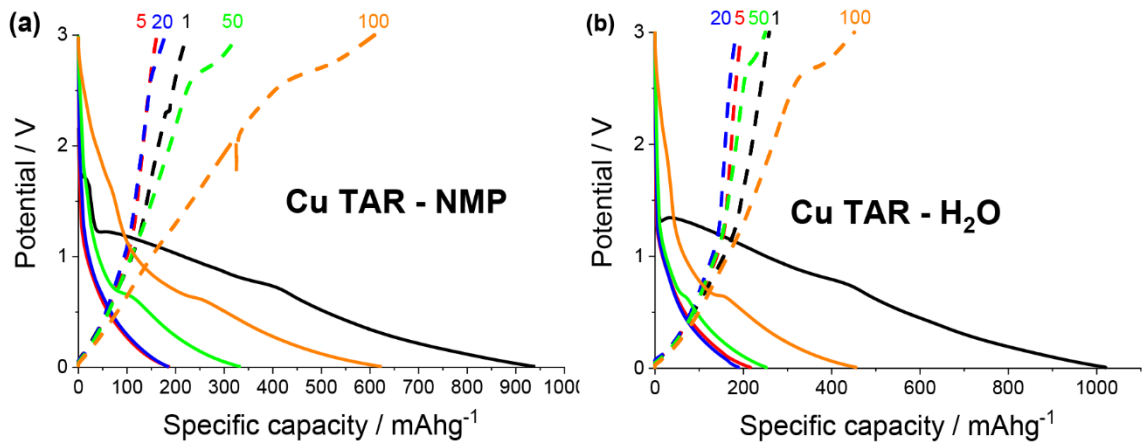

*Figure S3: Potential vs specific capacity curves for (a) NMP-based copper tartrate[9] and (b) water-based copper tartrate electrodes for cycles 1 (black), 5 (red), 20 (blue), 50 (green) and 100 (orange). All cycling was conducted at 50 $mAg^{-1}$ between 0.01 and 3 V.*

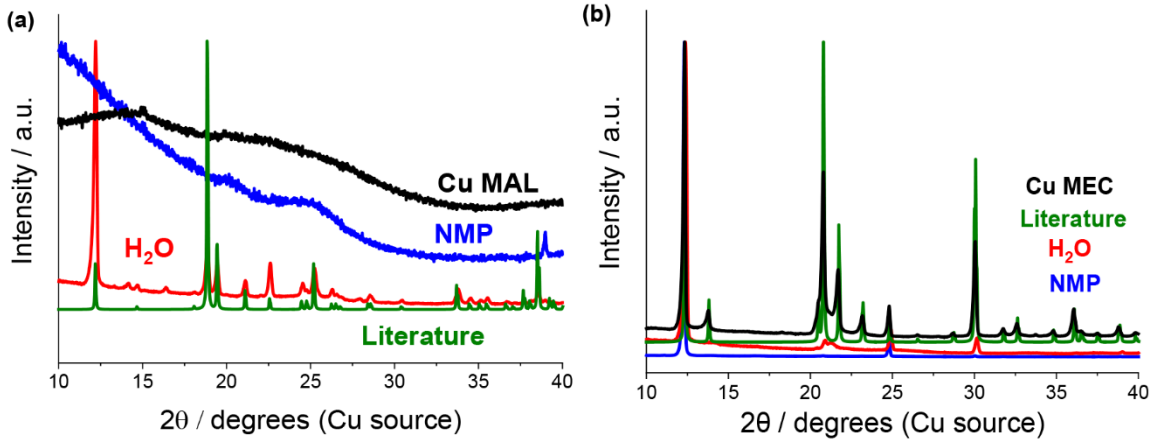


*Figure S4: XRD of synthesised (black) and literature comparison (green) copper-acid species and of NMP-based (blue) and water based electrodes (red) made from the copper-acid for (a) copper malate and (b) copper maleate. Literature copper malate and maleate patterns are from ICDD entries 00-052-1942 and 00-049-2453 respectively.*

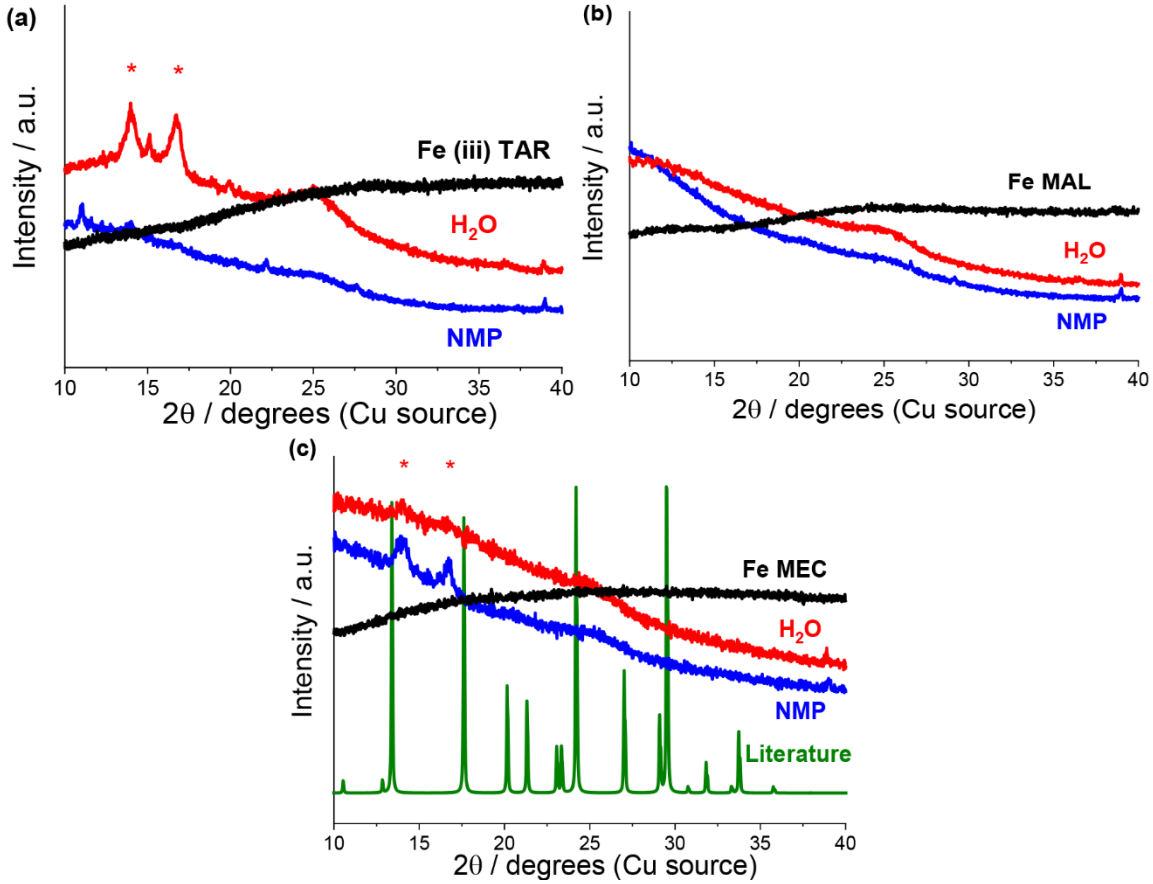


*Figure S5: XRD of synthesised (black) and literature comparison (green) iron-acid species and of NMP-based (blue) and water based electrodes (red) made from the iron-acid for (a) iron (iii) tartrate, (b) iron malate and (c) iron maleate. Red asterisk denotes peaks from adhesive used to hold sample. Literature iron maleate pattern is from ICDD entry 00-035-1710.*

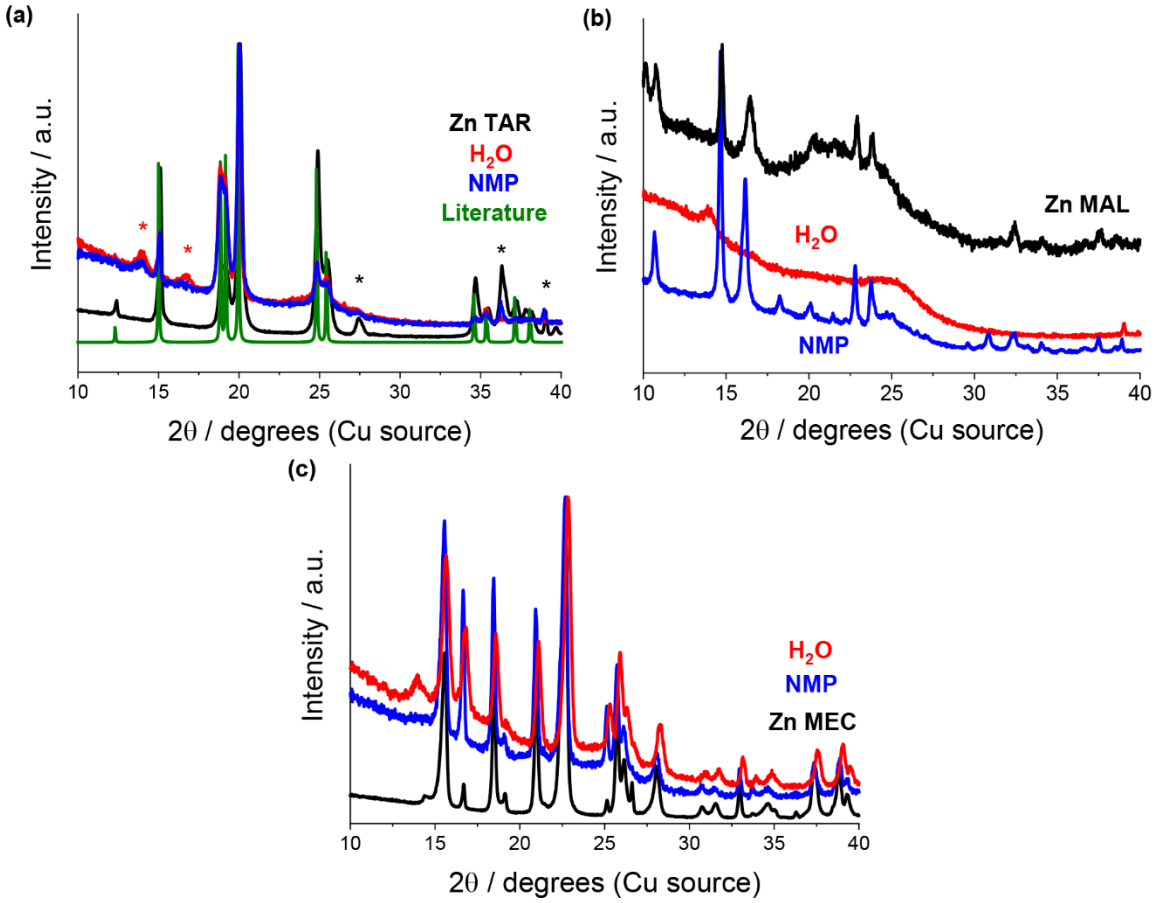


*Figure S6: XRD of synthesised (black) and literature comparison (green) zinc-acid species and of NMP-based (blue) and water based electrodes (red) made from the zinc-acid for (a) zinc tartrate, (b) zinc malate and (c) zinc maleate/succinate. Red asterisk denotes peaks from adhesive used to hold sample. Black asterisk denotes unaccounted for peaks. Literature zinc tartrate pattern is from ICDD entry 00-053-1692.*

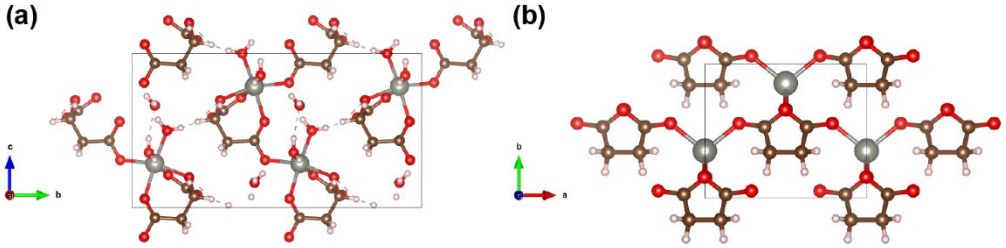


*Figure S7: SC XRD visualisation of synthesised (a) zinc malate and (b) zinc succinate. See Table S2 for crystallographic information.*

*Table S2: Crystallographic data for the synthesised copper tartrate hydrous, zinc malate and zinc succinate.*

| **Compound** | **Cu TAR Hydrous** | **Zn MAL** | **Zn SUC** |
|---|---|---|---|
| **CCDC number** | 927768 | 2234180 | 2234181 |
| **Formula** | $C_8H_{20}Cu_2O_{18}$ | $C_4H_{10}O_8Zn$ | $C_4H_4O_4Zn$ |
| **MM / gmol$^{-1}$** | 531.329 | 251.49 | 181.44 |
| **Crystal system** | Monoclinic | Monoclinic | Monoclinic |
| **Space group** | P 1 21 1 | C 1 c 1 | C 1 2 1 |
| **a / Å** | 8.3556(5) | 5.7928(3) | 7.5865(3) |
| **b / Å** | 8.7387(5) | 16.5335(8) | 5.9638(3) |
| **c / Å** | 12.0446(7) | 8.7909(4) | 6.2422(3) |
| **α / °** | 90 | 90 | 90 |
| **β / °** | 104.103(2) | 95.811(2) | 108.423(2) |
| **γ / °** | 90 | 90 | 90 |
| **V / Å$^3$** | 852.95(9) | 837.62(7) | 267.95(2) |
| **Z** | 2 | 4 | 2 |

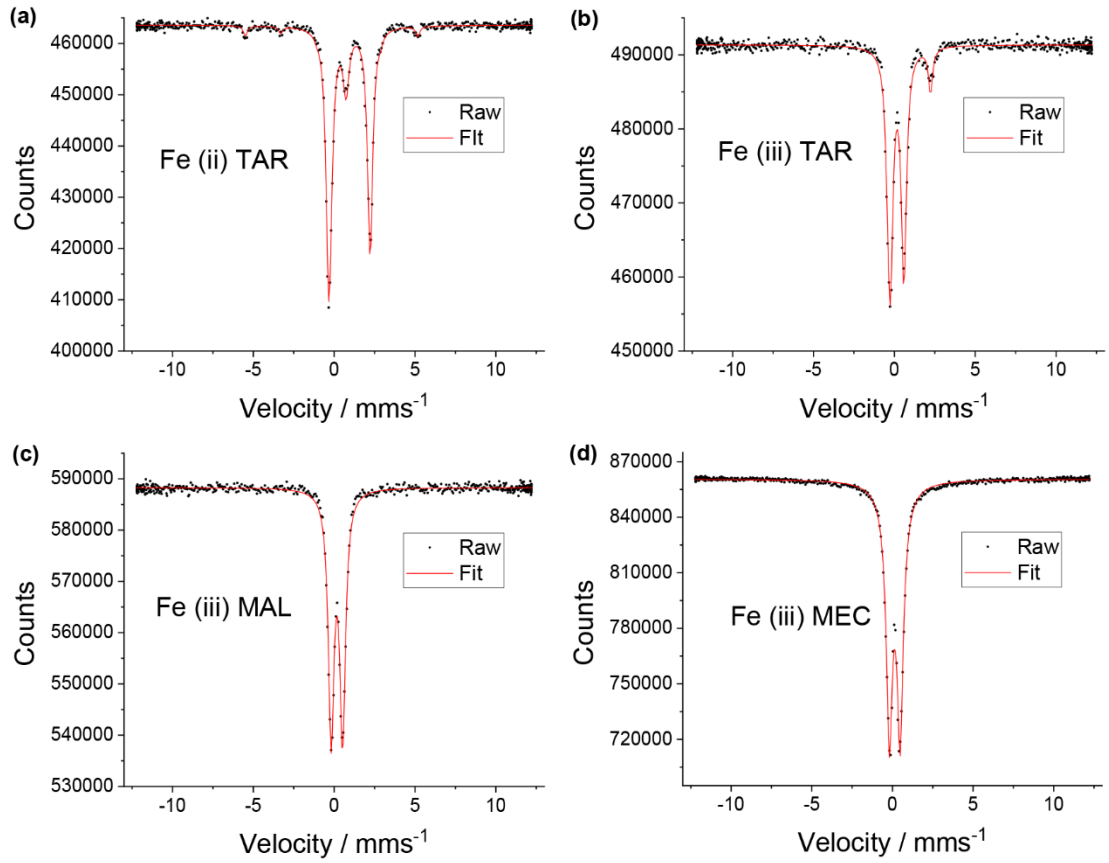


*Figure S8: Raw (black) and fitted (red) Mossbauer data for (a) iron (ii) tartrate, (b) iron (iii) tartrate, (c) iron (iii) malate and (d) iron (iii) maleate.*

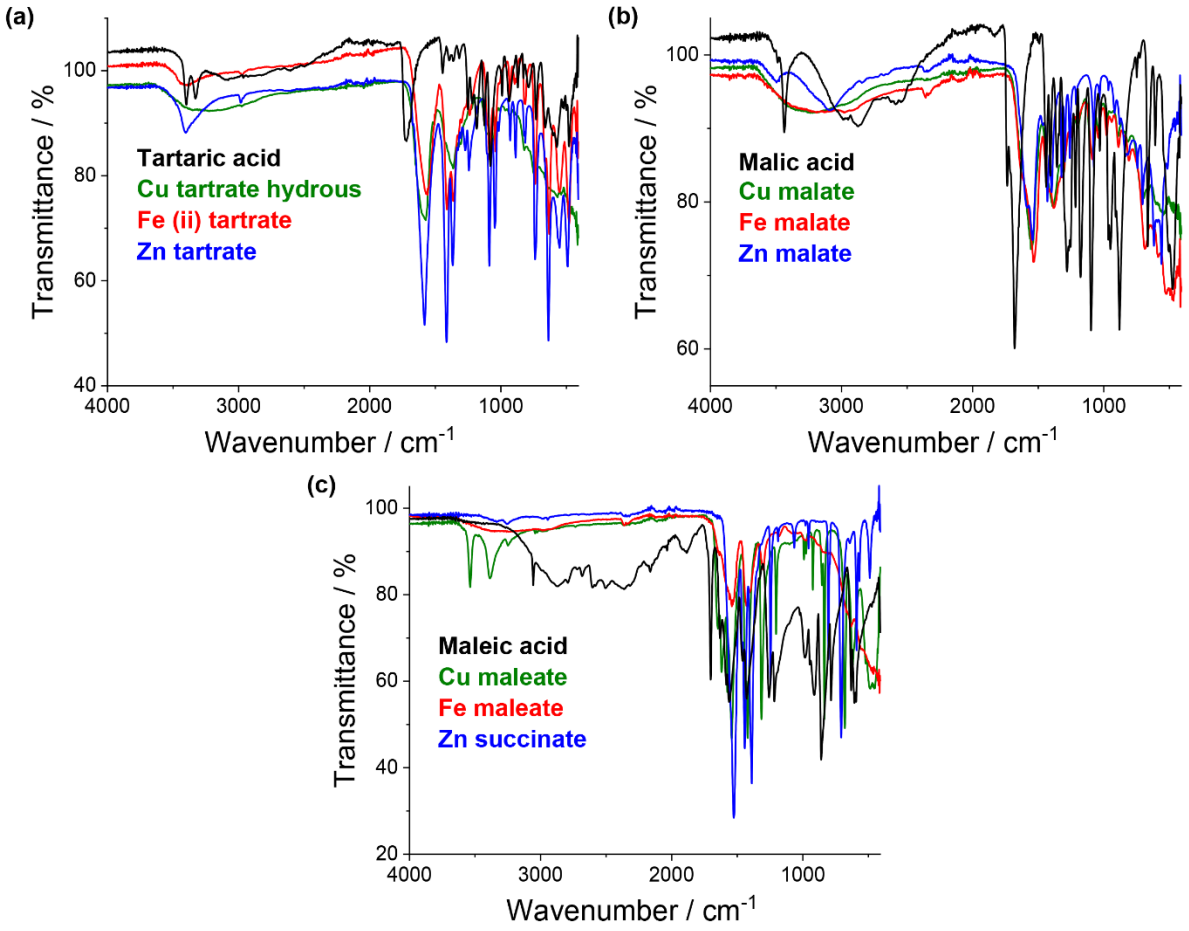


*Figure S9: FTIR spectra of precursor acid and synthesised compounds. (a) tartaric acid (black), copper tartrate hydrous (green), iron (ii) tartrate (red) and zinc tartrate (blue), (b) Malic acid (black), copper malate (green), iron malate (red), and zinc malate (blue) and (c) maleic acid (black), copper maleate (green), iron maleate (red), and zinc succinate (blue).*

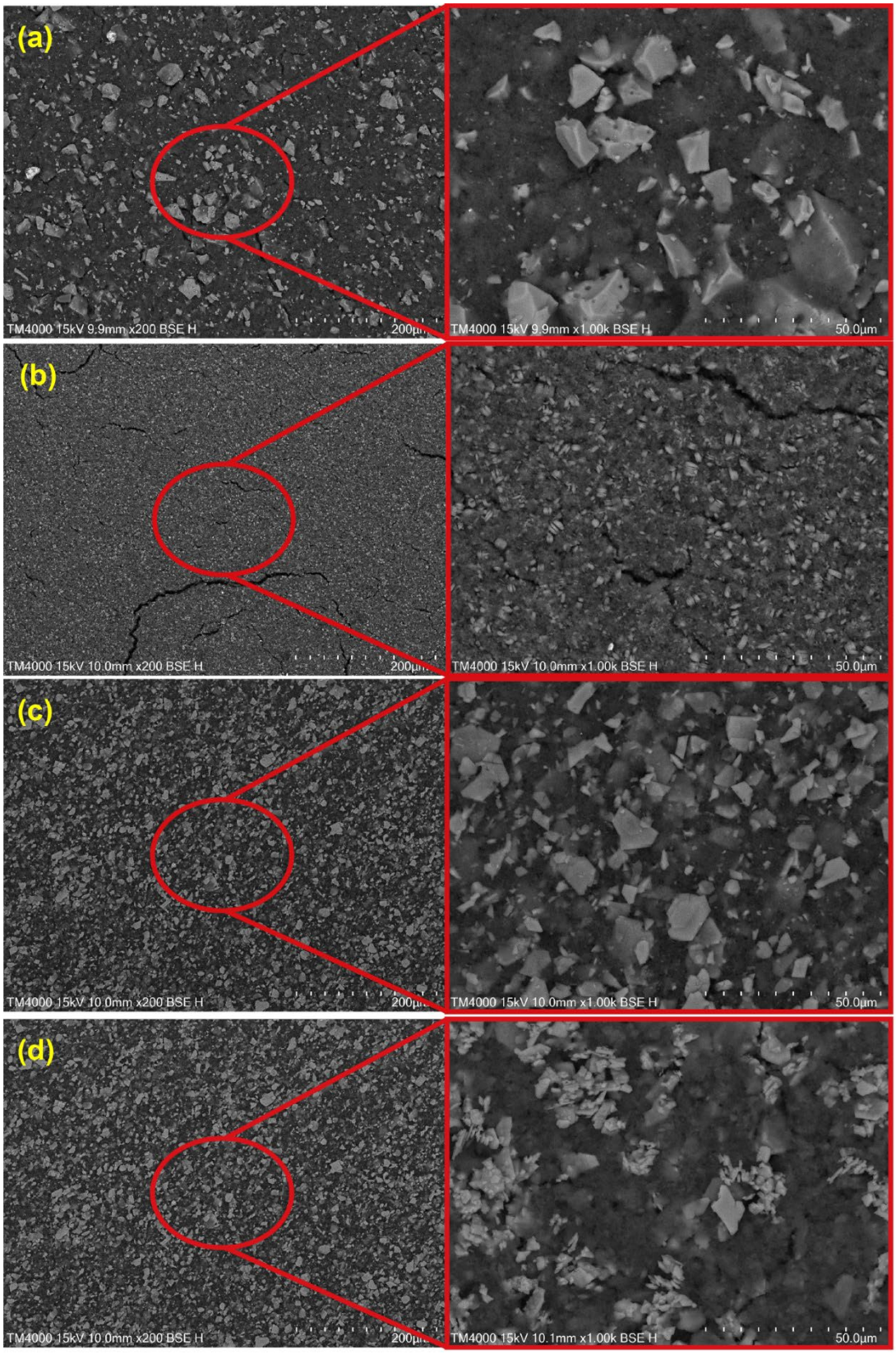
(a)
TM4000 15kV 9.9mm x200 BSE H
TM4000 15kV 9.9mm x1.00k BSE H
50.0µm
(b)
TM4000 15kV 10.0mm x200 BSE H
TM4000 15kV 10.0mm x1.00k BSE H
50.0µm
(c)
TM4000 15kV 10.0mm x200 BSE H
TM4000 15kV 10.0mm x1.00k BSE H
50.0µm
(d)
TM4000 15kV 10.0mm x200 BSE H
TM4000 15kV 10.1mm x1.00k BSE H
50.0µm

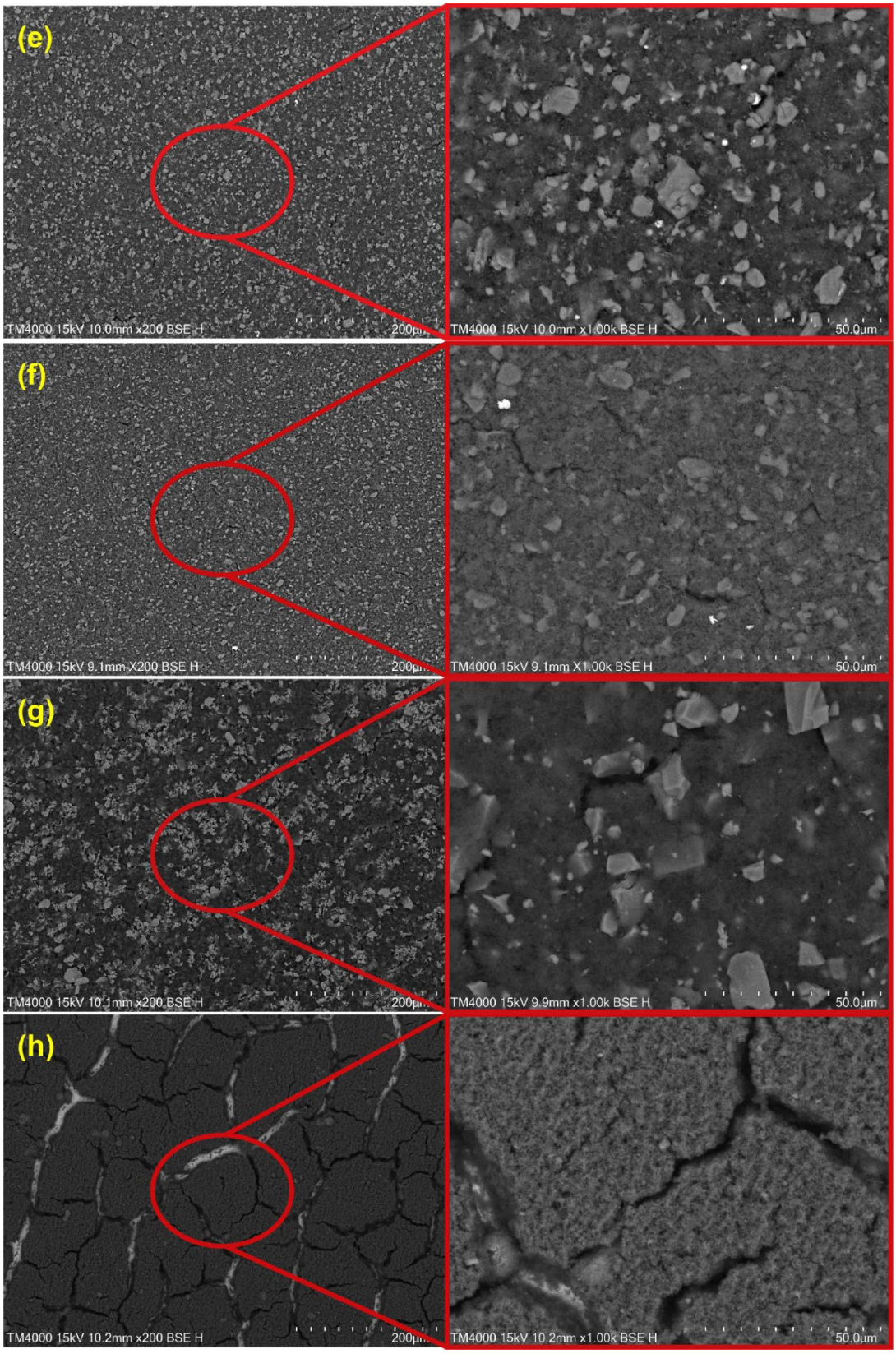
(e)
TM4000 15kV 10.0mm x200 BSE H
TM4000 15kV 10.0mm x1.00k BSE H
50.0µm
(f)
TM4000 15kV 9.1mm X200 BSE H
TM4000 15kV 9.1mm X1.00k BSE H
50.0µm
(g)
TM4000 15kV 10.1mm x200 BSE H
TM4000 15kV 9.9mm x1.00k BSE H
50.0µm
(h)
TM4000 15kV 10.2mm x200 BSE H
TM4000 15kV 10.2mm x1.00k BSE H
50.0µm

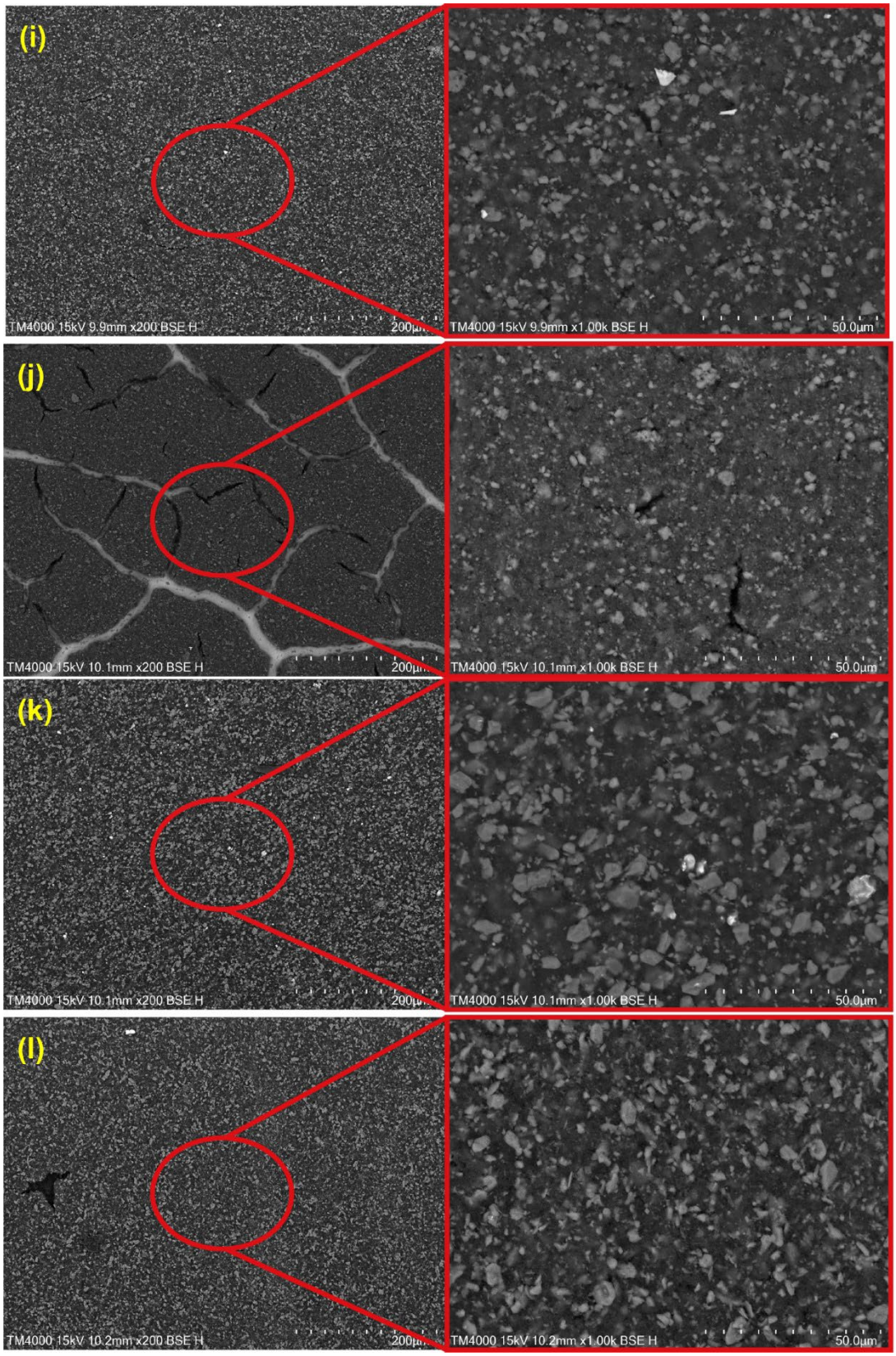
(i)
TM4000 15kV 9.9mm x200 BSE H
200µm
TM4000 15kV 9.9mm x1.00k BSE H
50.0µm
(j)
TM4000 15kV 10.1mm x200 BSE H
200µm
TM4000 15kV 10.1mm x1.00k BSE H
50.0µm
(k)
TM4000 15kV 10.1mm x200 BSE H
200µm
TM4000 15kV 10.1mm x1.00k BSE H
50.0µm
(l)
TM4000 15kV 10.2mm x200 BSE H
200µm
TM4000 15kV 10.2mm x1.00k BSE H
50.0µm

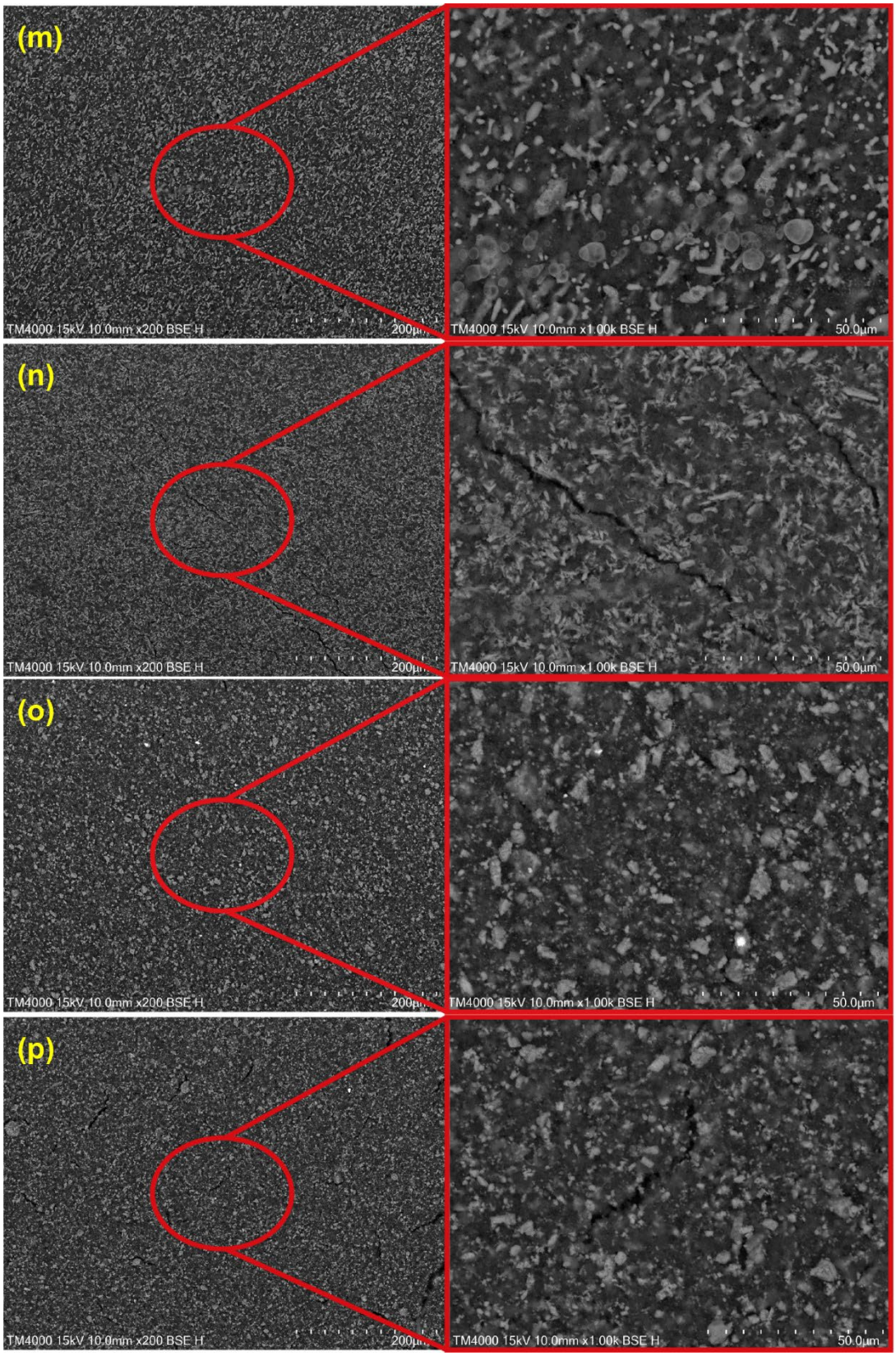


*Figure S10: SEM (200/1000x, 15 kV) of pristine NMP and $H_2O$ electrodes. (a) Cu MAL – NMP, (b) Cu MAL – $H_2O$, (c) Cu MEC – NMP, (d) Cu MEC – $H_2O$, (e) Fe (ii) TAR – NMP, (f) Fe (ii) TAR – $H_2O$, (g) Fe (iii) TAR – NMP, (h) Fe (iii) TAR – $H_2O$, (i) Fe MEC – NMP, (j) Fe MEC – $H_2O$, (k) Zn TAR – NMP, (l) Zn TAR – $H_2O$, (m) Zn MAL – NMP, (n) Zn MAL – $H_2O$, (o) Zn MEC – NMP, (p) Zn MEC – $H_2O$.*

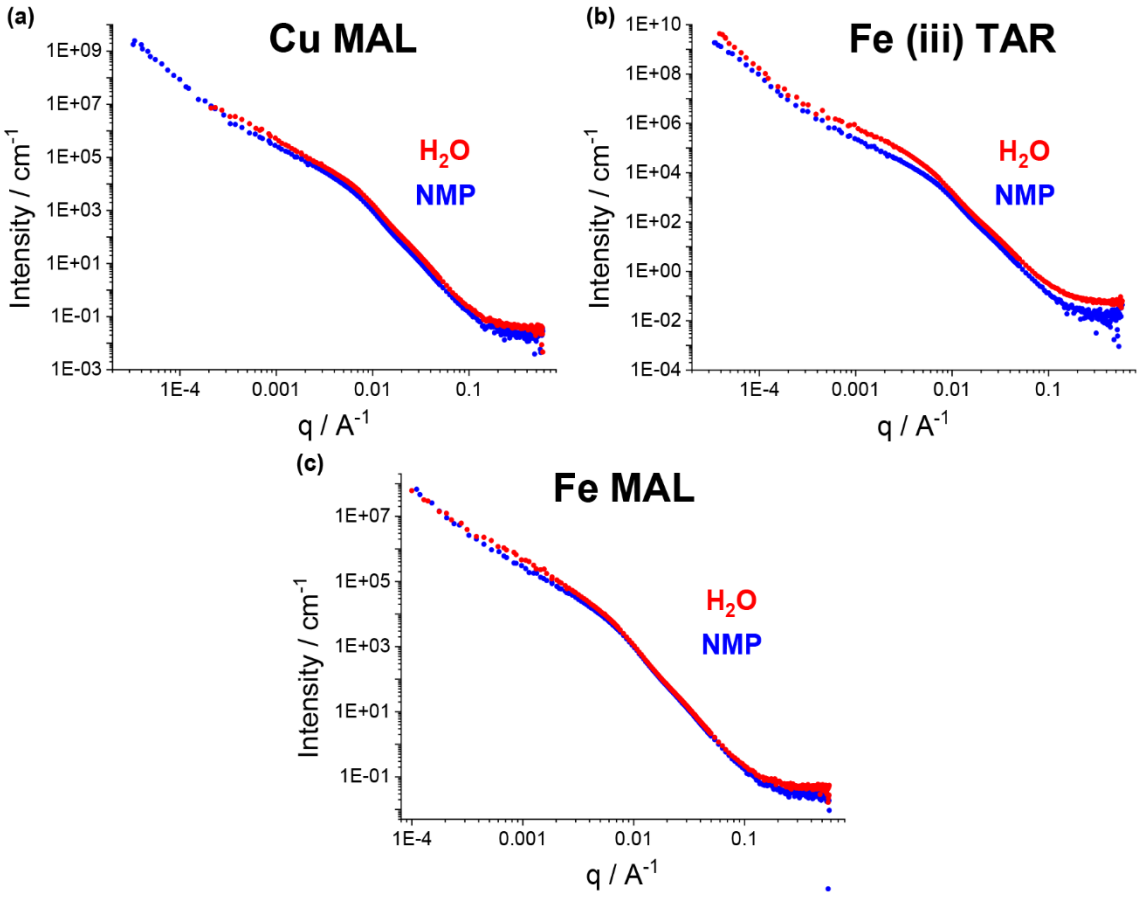


*Figure S11: SANS and USANS data NMP-based (blue) and $H_2O$-based (red) metal-acid electrodes. (a) copper malate, (b) iron (iii) tartrate, and (c) iron malate.*

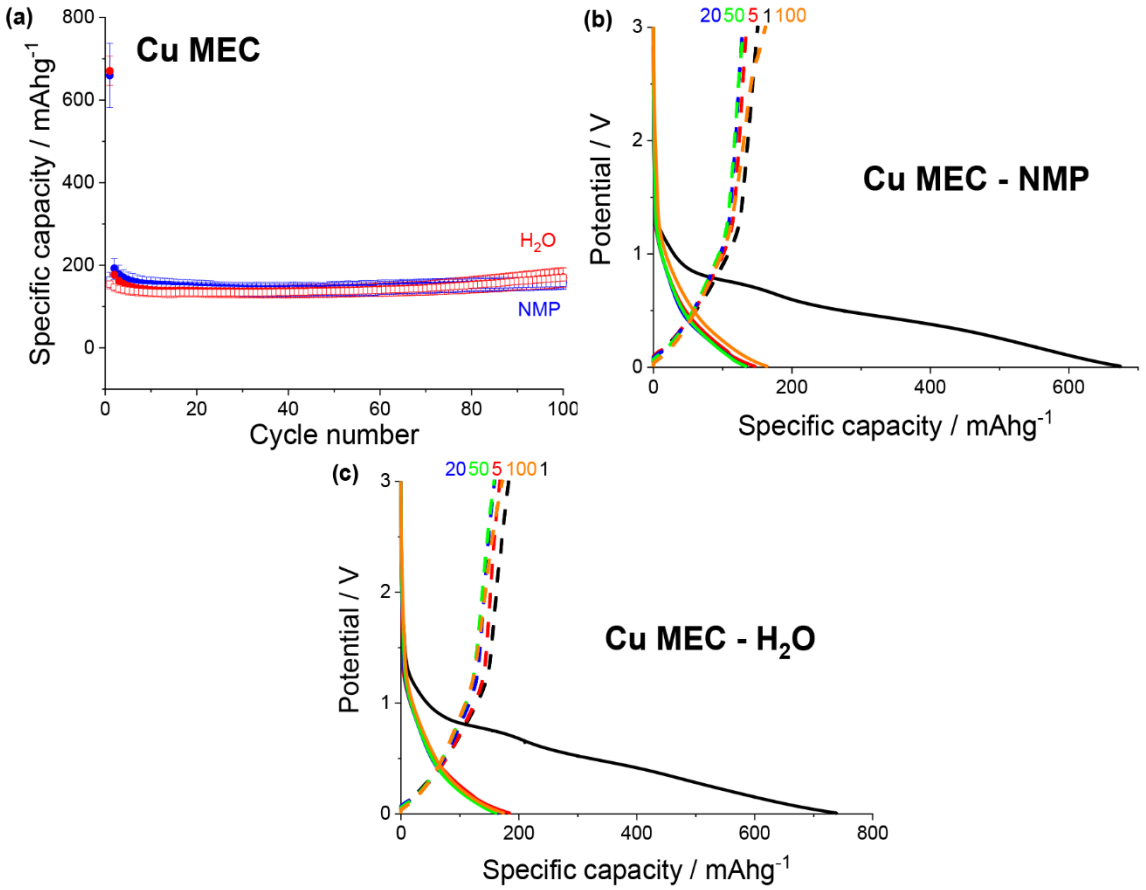


*Figure S12: (a) Discharge (filled) and charge (non-filled) specific capacity vs cycle number for NMP-based (blue) and water-based (red) copper maleate electrodes. Potential vs specific capacity curves for (b) NMP-based copper maleate and (c) water-based copper maleate electrodes, for cycles 1 (black), 5 (red), 20 (blue), 50 (green) and 100 (orange). All cycling was conducted at 50 $mAg^{-1}$ between 0.01 and 3 V.*

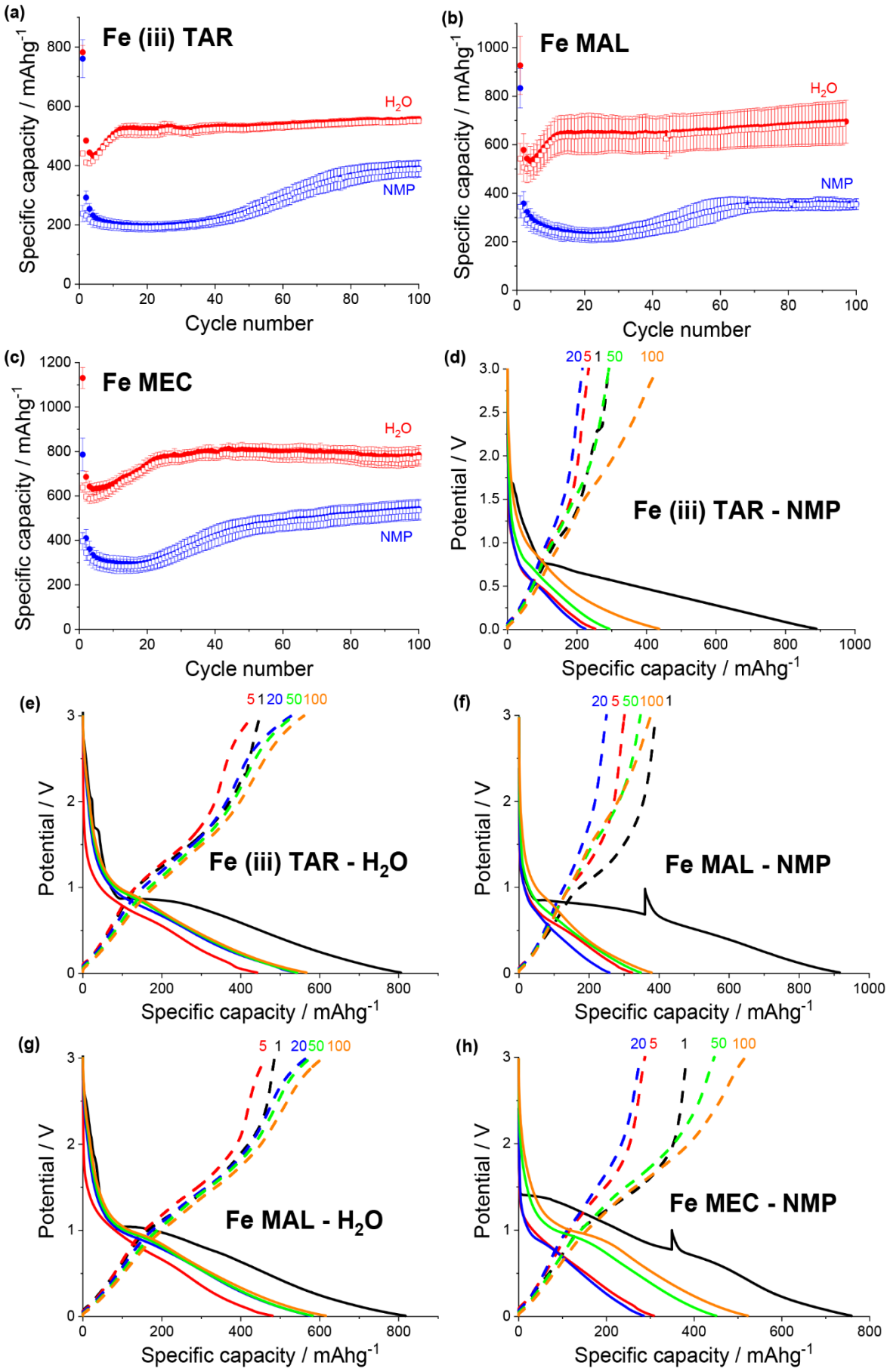
(a)
Fe (iii) TAR
Specific capacity / mAhg-1
Cycle number
H2O
NMP
(b)
Fe MAL
Specific capacity / mAhg-1
Cycle number
H2O
NMP
(c)
Fe MEC
Specific capacity / mAhg-1
Cycle number
H2O
NMP
(d)
20 5 1 50 100
Fe (iii) TAR - NMP
Potential / V
Specific capacity / mAhg-1
(e)
5 1 20 50 100
Fe (iii) TAR - H2O
Potential / V
Specific capacity / mAhg-1
(f)
20 5 50 100 1
Fe MAL - NMP
Potential / V
Specific capacity / mAhg-1
(g)
5 1 20 50 100
Fe MAL - H2O
Potential / V
Specific capacity / mAhg-1
(h)
20 5 1 50 100
Fe MEC - NMP
Potential / V
Specific capacity / mAhg-1

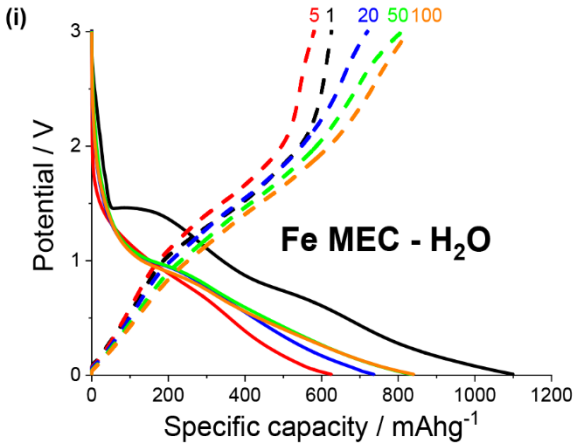


*Figure S13: Discharge (filled) and charge (non-filled) specific capacity vs cycle number for NMP-based (blue) and water-based (red) electrodes for (a) iron (iii) tartrate, (b) iron malate and (c) iron maleate. Potential vs specific capacity curves for (d) NMP-based iron (iii) tartrate, (e) water-based iron (iii) tartrate, (f) NMP-based iron malate, (g) water-based iron malate, (h) NMP-based iron maleate and (i) water-based iron maleate electrodes, for cycles 1 (black), 5 (red), 20 (blue), 50 (green) and 100 (orange). All cycling was conducted at 50 $mAg^{-1}$ between 0.01 and 3 V.*

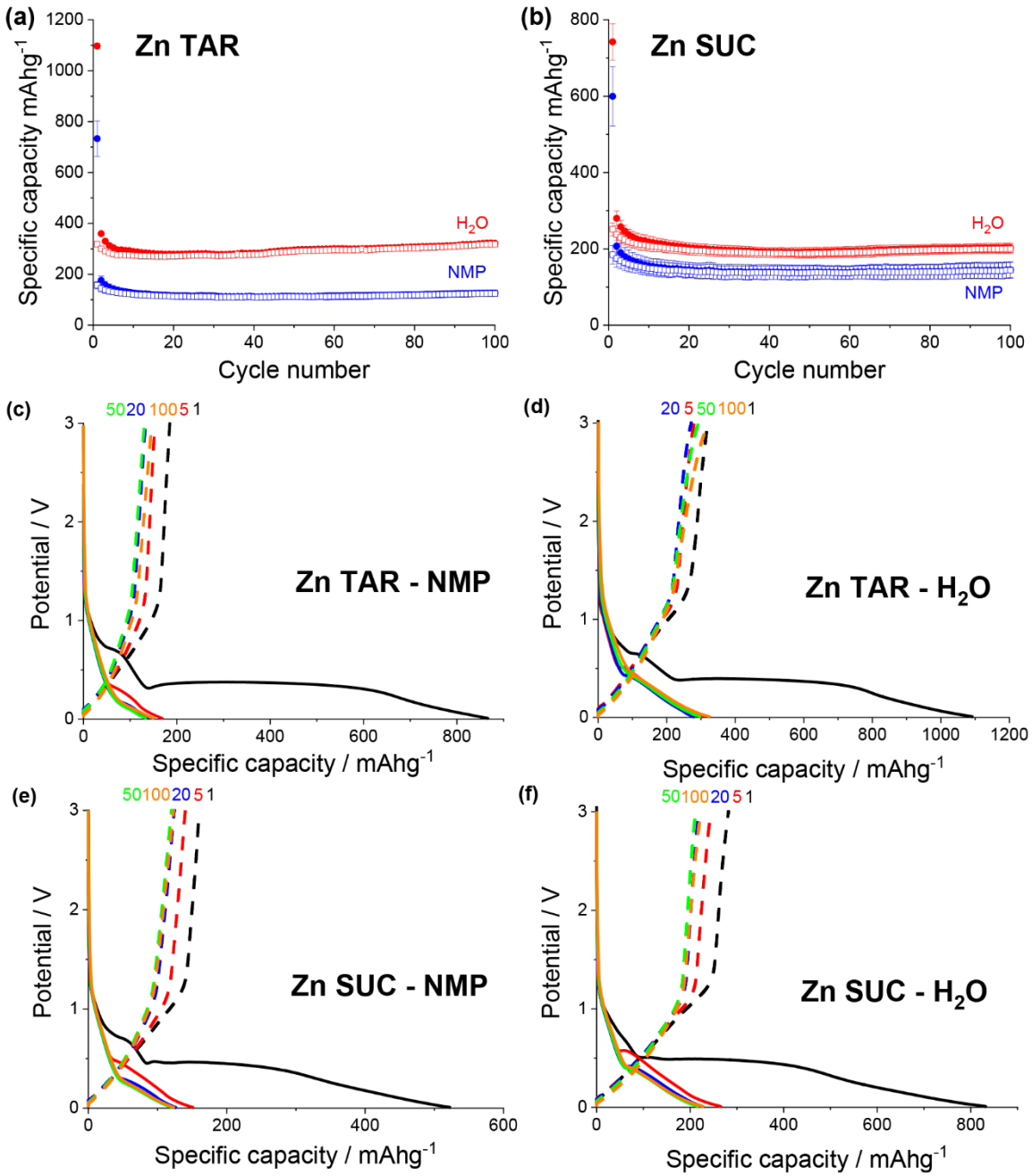


*Figure S14: Discharge (filled) and charge (non-filled) specific capacity vs cycle number for NMP-based (blue) and water-based (red) electrodes for (a) zinc tartrate, and (b) zinc succinate. Potential vs specific capacity curves for (c) NMP-based zinc tartrate, (d) water-based zinc tartrate, (e) NMP-based zinc succinate, and (f) water-based zinc succinate, for cycles 1 (black), 5 (red), 20 (blue), 50 (green) and 100 (orange). All cycling was conducted at 50 $mAg^{-1}$ between 0.01 and 3 V.*

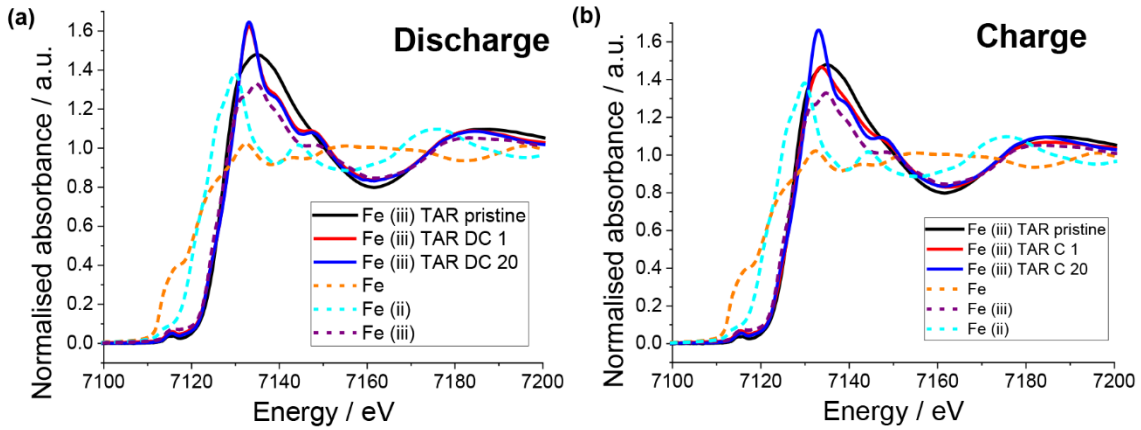


*Figure S15: XAS of pristine and cycled (vs Li) iron (iii) tartrate electrodes. (a) Discharged to 0.01 V and (b) charged to 3 V at 50 $mAg^{-1}$.*

# References


1. Bruker *SAINT and SADABS*, Bruker AXS Inc: Madison, Wisconsin, USA, 2016.
2. Sheldrick, G., SHELXT - Integrated space-group and crystal-structure determination. *Acta Crystallographica Section A* **2015,** *71* (1), 3-8.
3. Sheldrick, G., Crystal structure refinement with SHELXL. *Acta Crystallographica Section C* **2015,** *71* (1), 3-8.
4. Dolomanov, O. V.; Bourhis, L. J.; Gildea, R. J.; Howard, J. A. K.; Puschmann, H., OLEX2: a complete structure solution, refinement and analysis program. *Journal of Applied Crystallography* **2009,** *42* (2), 339-341.
5. Wood, K.; Mata, J. P.; Garvey, C. J.; Wu, C.-M.; Hamilton, W. A.; Abbeywick, P.; Bartlett, D.; Bartsch, F.; Baxter, P.; Booth, N.; Brown, W.; Christoforidis, J.; Clowes, D.; d'Adam, T.; Darmann, F.; Deura, M.; Harrison, S.; Hauser, N.; Horton, G.; Federici, D.; Franceschini, F.; Hanson, P.; Imamovic, E.; Imperia, P.; Jones, M.; Kennedy, S.; Kim, S.; Lam, T.; Lee, W. T.; Lesha, M.; Mannicke, D.; Noakes, T.; Olsen, S. R.; Osborn, J. C.; Penny, D.; Perry, M.; Pullen, S. A.; Robinson, R. A.; Schulz, J. C.; Xiong, N.; Gilbert, E. P., QUOKKA, the pinhole small-angle neutron scattering instrument at the OPAL Research Reactor, Australia: design, performance, operation and scientific highlightsThis article will form part of a virtual special issue on advanced neutron scattering instrumentation, marking the 50th anniversary of the journal. *Journal of Applied Crystallography* **2018,** *51* (2), 294-314.
6. Rehm, C.; de Campo, L.; Brule, A.; Darmann, F.; Bartsch, F.; Berry, A., Design and performance of the variable-wavelength Bonse-Hart ultra-small-angle neutron scattering diffractometer KOOKABURRA at ANSTOThis article will form part of a virtual special issue on advanced neutron scattering instrumentation, marking the 50th anniversary of the journal. *Journal of Applied Crystallography* **2018,** *51* (1), 1-8.
7. Kline, S. R., Reduction and analysis of SANS and USANS data using IGOR Pro. *Journal of Applied Crystallography* **2006,** *39* (6), 895-900.
8. Ravel, B.; Newville, M., ATHENA, ARTEMIS, HEPHAESTUS: data analysis for X-ray absorption spectroscopy using IFEFFIT. *Journal of Synchrotron Radiation* **2005,** *12* (4), 537-541.
9. Teusner, M.; Mittal, U.; Lessio, M.; Johannessen, B.; Mata, J.; Sharma, N., Formulation and mechanism of copper tartrate - an anode material for lithium-ion batteries - under review. **2022**.
10. Teusner, M.; Mata, J.; Sharma, N., In situ synthesis of Cu (ii) dicarboxylate MOFs and their application as battery materials - under review. **2022**.